


Imperial College London

# *Chiral-Induced Spin Selectivity Film on a Superconducting Surface*



| | |
|---|---|
| **Group members** | **Shahad Alrifai, Muzun Almahmoud, and Nisrin Balhareth** |
| **Project mentor** | **Dr. Niladri Banerjee** |
| **Internship institution** | **Imperial College London** |

# Abstract

In recent years, increasing attention has been devoted to the role of chirality in molecular systems, extending beyond structural aspects to include unique electronic properties. Electrons that pass through chiral molecules, or even charge displacements within a chiral molecule, occur in a manner that depends on the electron's spin and the molecule's enantiomeric form. In this work, we fabricated a chiral thin film and investigated its superconducting properties. We therefore reasoned that the induced spin polarization may affect electron transport in superconductors, which may not rely on the conventional Cooper pair formation. This mechanism, rooted in spin-selective interactions induced by molecular chirality, may pave the way for new directions in the design and development of next-generation superconducting materials.

## Acknowledgment

We would like to express our sincere gratitude to God for granting us the strength and guidance to successfully complete this training. Our heartfelt thanks go to KAUST Academy, the Women and Energy Association, and King Abdullah City for Atomic and Renewable Energy (K•A•CARE) for launching and supporting this program, and for investing in the future of women in energy. We are also grateful to our training supervisor at Imperial College London, Dr. Niladri Banerjee, for his valuable mentorship, continuous support, and insightful guidance throughout this experience. Finally, we thank Imperial College London for hosting us as part of the WE Spark program, which is dedicated to developing and empowering Saudi women in the energy sector.

# Contents

Abstract ..... I

Acknowledgment ..... II

1.Introduction ..... 1

2.Project objectives ..... 2

3.Methodology ..... 3

3.1 Simulated Equilibrium Distribution of SAM Layers on a Rough Gold Surface ..... 3

3.2 Thin-Film Coating ..... 5

4. Results and Dissection ..... 6

4.1 Peptide Characterization ..... 6

4.1.1 Mass Spectrum ..... 6

4.1.2 UV-Vis Spectroscopy ..... 7

4.2 Thin-Film Characterization ..... 8

4.2.1 Simulation of SAM Distribution ..... 8

4.2.2 Atomic Force Microscopy (AFM) ..... 9

4.2.3 Physical Property Measurement System (PPMS) ..... 11

5. Challenges and Future ..... 14

6. Resources and Tools ..... 14

7. Reference ..... 16

# 1.Introduction

The chiral-induced spin selectivity (CISS) effect refers to the preferential transmission of electrons with one spin orientation through chiral molecules or structures (Figure 1a, b). This spin filtering that occurs without external magnetic fields stems from the coupling of an electron's spin to its motion in a chiral electrostatic potential. CISS has been demonstrated in a wide range of systems and underpins phenomena from long-range electron transfer in biology to emerging spintronic technologies.[1][2].

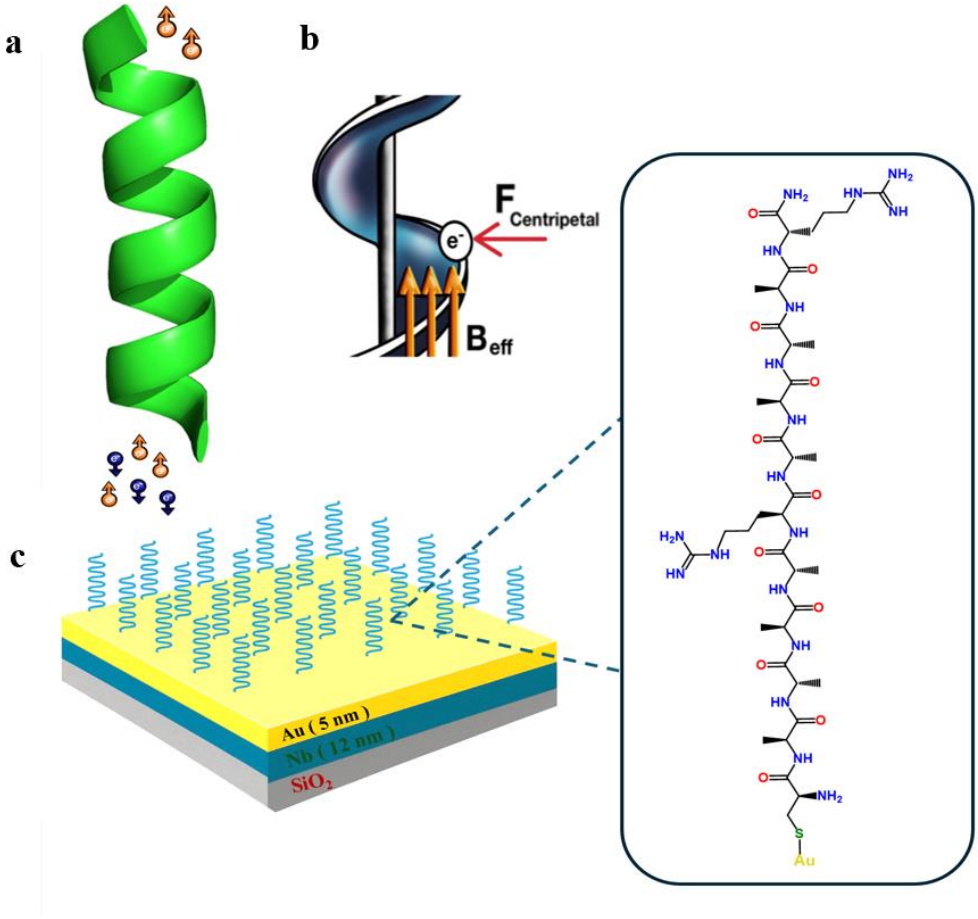



**Figure 1. (a) A scheme of the proposed chiral induced spin selectivity (CISS) mechanism. (b) The spin-dependent charge reorganization (SDCR). (C) Schematic illustration of the Nb/Au surface modified with a chiral molecular.**

Building on these insights, recent studies have explored the role of CISS in superconductivity. Conventional s-wave superconductors such as lead exhibit spin-singlet pairing that is highly sensitive to magnetic fields, so introducing chiral molecular layers on superconducting surfaces can modify this behavior, broadening the superconducting transition and increasing the critical field under in-plane fields [3]. These findings open pathways for superconducting spintronics, where chirality serves as a tool to locally control superconducting properties.

In this project, we investigated how a CISS film interacts with a superconducting surface by depositing peptide chiral molecules onto Nb/Au substrates (Figure 1c). By comparing the structural and functional characteristics of these films before and after the substrate entered the superconducting state, we aimed to assess the influence of molecular chirality on superconducting behavior and surface properties.

## 2.Project objectives

Our main objective for this project was to understand the CISS effect and explore the impact of applying a chiral molecule on a superconductor. In order to do so, we needed to gain experience in characterizing materials using atomic force microscopy (AFM) and in interpreting the results obtained from the physical property measurement system (PPMS). Once these skills were acquired, we also aimed to visualize and analyze the data using various software tools.

We sought to investigate how substrate morphology and surface roughness influence the formation of self-assembled monolayers (SAMs), employing a simulation framework based on the Boltzmann distribution together with an energy model describing the gold–sulfur binding dependence on the adsorption angle ($\cos\theta$).

# 3.Methodology

## 3.1 Simulated Equilibrium Distribution of SAM Layers on a Rough Gold Surface

The model considers the variation of effective binding energy due to the roughness which affects the adsorption density. To model the roughness, we have assumed a Gaussian-type height fluctuation where the height at each point (x,y) is denoted by z(x,y) and has the form of a normal distribution. The mean is set at zero which is the surface about which the height fluctuates with a standard deviation of 1 nm (RMS roughness).

$$P(z) = \frac{1}{\sqrt{2\pi\,(1)^2}} \exp\left(-\frac{z^2}{2}\right)$$

To create the rough surface, we created a grid of points 100 x 100 and to each point I assigned a z value which is sampled from this distribution which in python reads:

*rough_surface = np.random.normal(loc=0.0, scale=1.0, size=(100, 100)).*

The overall surface has zero mean height and 1 nm RMS roughness (which will be varied later in simulation).

The local slope at each point can be calculated by using:

$$\text{Slope}\,(x,y) = \sqrt{\left(\frac{\partial z}{\partial x}\right)^2 + \left(\frac{\partial z}{\partial y}\right)^2}$$

Now from this slope we can calculate the local tilt angle which is defined as the angle between the local surface normal and the z axis:

$$\theta(x,y) = \arctan\left(\text{slope}(x,y)\right)$$

The local binding energy should depend on this surface tilt for two reasons:

1. **Steric Hindrance:**
- Molecules always align their long axis with the local surface normal.
- On a rough surface, neighboring molecules may tilt towards each other.

- This reduces effective binding probability → modeled as lower binding energy.

**2. Au Coordination Effect:**

- At sharp peaks, Au atoms have reduced coordination numbers.
- This alters the Au–S binding energy.

So we have bundled everything in this position dependent binding energy term with a cosine dependence.

$$E_{bind}(x,y) = E_0 \cos(\theta(x,y))$$

From Jeremy Baumberg's paper[4], we got $E_0$ as 1.95 eV on flat Au.

Now the equilibrium density is determined by a Boltzmann distribution:

$$\rho_{unnorm}(x,y) \propto \exp\left(\frac{E_{bind}(x,y)}{K_B T}\right)$$

The molecular packing density from Harry's paper [5], $\rho_{peptide}$ =10 molecules/nm$^2$

$$\rho_{norm}(x,y) = \rho_{unnorm}(x,y) \times \left(\frac{\rho_{peptide}}{<\rho_{unnorm}>}\right)$$

So, finally we plot

$$\rho_{norm}(x,y) = \exp\left(\frac{E_{bind}(x,y)}{K_B T}\right) \times \left(\frac{\rho_{peptide}}{<\exp\left(\frac{E_{bind}(x,y)}{K_B T}\right)>}\right)$$

Python code for this:

```
rho_unnorm = np.exp(E_bind_local / kB_T)

rho_mean = np.mean(rho_unnorm)

rho_surface = rho_unnorm * (packing_density / rho_mean)
```

## 3.2 Thin-Film Coating

Peptide thin films were fabricated on Nb/Au substrates using a standard spin-coating procedure. The synthesized peptide was first dissolved in methanol to prepare a homogeneous solution at the desired concentration. Prior to coating, the Nb/Au substrates were carefully cleaned with ethanol and deionized water, followed by drying under a nitrogen stream, in order to remove possible surface contaminants.

For the coating step, a controlled volume of the peptide–methanol solution was deposited dropwise onto the center of the substrate surface (Figure 2**,** step 1). Immediately afterwards, the substrate was rotated at high speed using a spin coater, which enabled uniform spreading of the solution over the entire surface by centrifugal force (Figure 2**,** step 2). The spinning speed and duration were optimized to achieve continuous coverage and to minimize film thickness variations across the sample.

During spinning, the methanol solvent gradually evaporated, resulting in the deposition of a thin, homogeneous peptide film on the Nb/Au surface (Figure 2**,** step 3). The thickness and surface morphology of the resulting films were subsequently examined by atomic force microscopy (AFM), while their functional and structural properties were further analyzed using complementary techniques described in later sections.

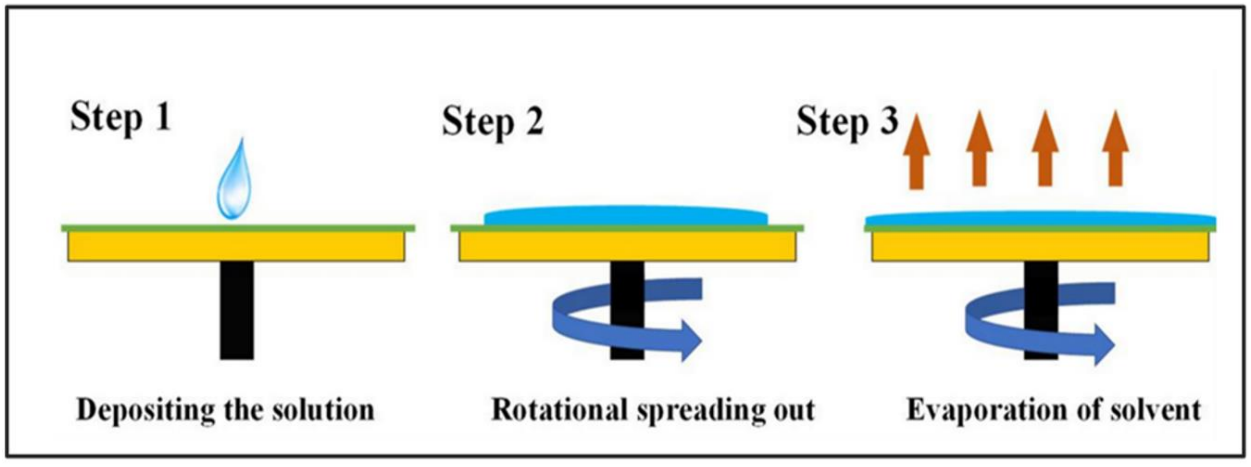



**Figure 2. The spin coating process. a) A solution of peptide in a common solvent is dropped onto the substrate.**

# 4. Results and Dissection

## 4.1 Peptide Characterization

### 4.1.1 Mass Spectrum

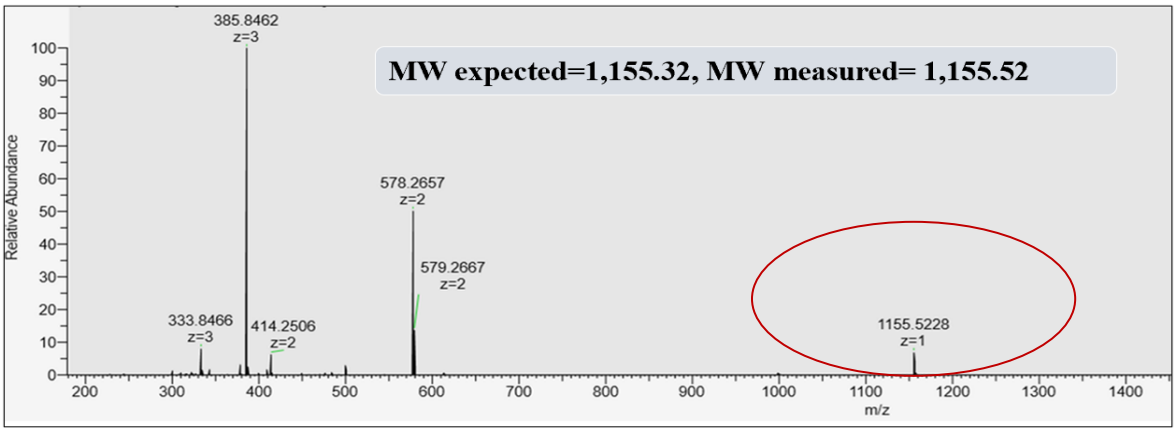



**Figure 3. The mass spectrum of the synthesized peptide.**

The mass spectrum of the synthesized peptide is presented in Figure 3. The expected molecular weight (MW) of the peptide was calculated to be 1,155.32 Da, while the measured molecular weight was found to be 1,155.52 Da, showing an excellent agreement between the theoretical and experimental values. The spectrum exhibits a major peak at m/z = 1155.52 (z = 1), which corresponds to the intact molecular ion of the peptide. Additional peaks observed at lower m/z values (e.g., 333.85, 385.84, 414.25, 578.27, 579.27) represent multiply charged species and fragment ions generated during ionization.

The close match between the calculated and measured molecular weights confirms the successful synthesis of the target peptide, and the presence of the molecular ion peak further validates its structural integrity.

### 4.1.2 UV-Vis Spectroscopy

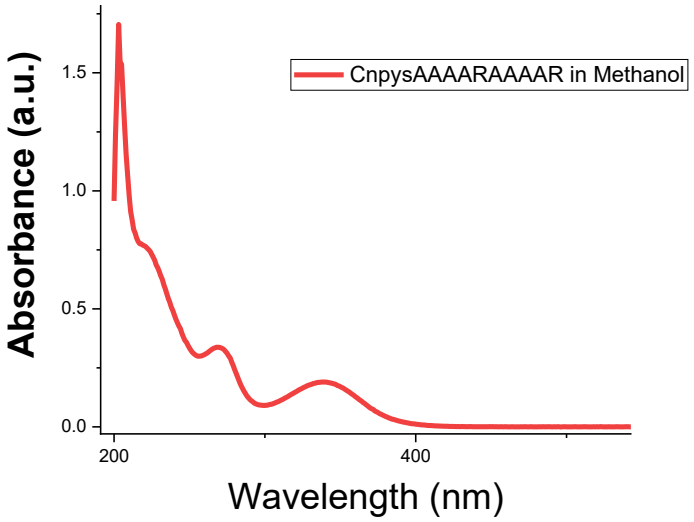



**Figure 4. UV–Vis absorption spectrum of the synthesized peptide in methanol.**

The UV–Vis absorption spectrum of the synthesized peptide (Figure 4) was recorded in methanol solution within the range of 200–600 nm. A strong absorption band was observed at approximately 200–220 nm, which is characteristic of the peptide backbone due to π–π* transitions of the amide bonds. The intensity of this peak indicates the presence of ordered peptide structures and confirms the solubility of the compound in the selected solvent. A weaker shoulder extending around 260–280 nm may be attributed to n–π* transitions associated with carbonyl groups in the peptide.

These results provide supporting evidence for the structural integrity of the synthesized peptide and complement the mass spectrometry findings.

## 4.2 Thin-Film Characterization

### 4.2.1 Simulation of SAM Distribution

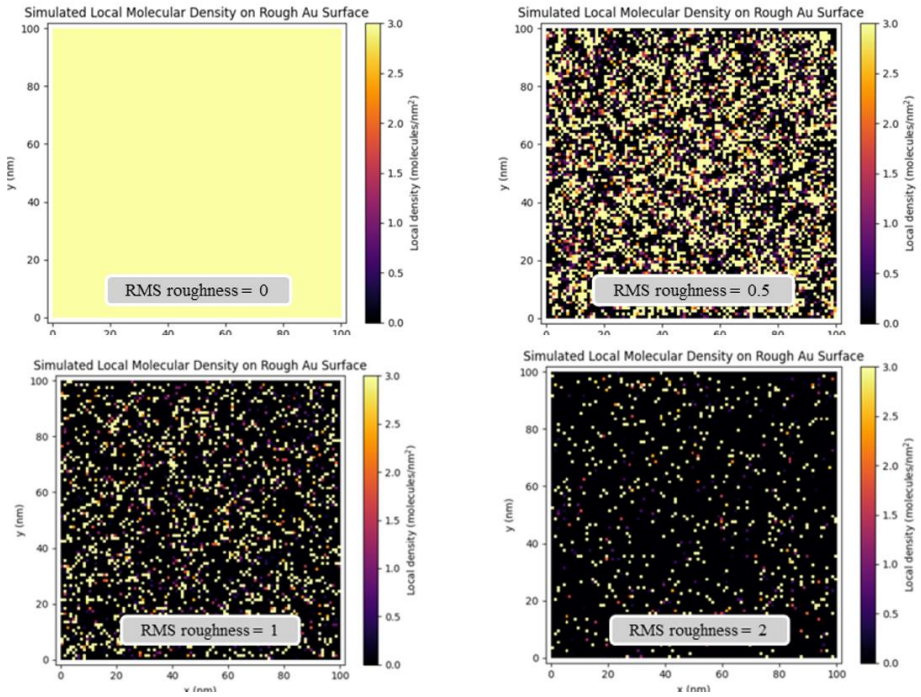



**Figure 5. Simulation of the effect of gold surface roughness on peptide distribution.**

Figure 5 illustrates the simulated effect of gold surface roughness on the distribution of peptide self-assembled monolayers (SAMs). At RMS roughness = 0, the surface appears highly uniform, resulting in a homogeneous distribution of peptide molecules with minimal clustering. When the roughness is slightly increased (RMS = 0.5), localized variations begin to appear, leading to small regions of higher molecular density.

As the roughness increases further (RMS = 1 and 2), the simulations show a progressively more heterogeneous distribution, with peptides aggregating preferentially at valleys and irregular regions of the gold surface. This behavior indicates that surface morphology plays a significant role in peptide adsorption and spatial organization.

These results suggest that controlling the nanoscale roughness of gold substrates can be a key factor in tuning the uniformity and functional properties of peptide-based thin films.

### 4.2.2 Atomic Force Microscopy (AFM)

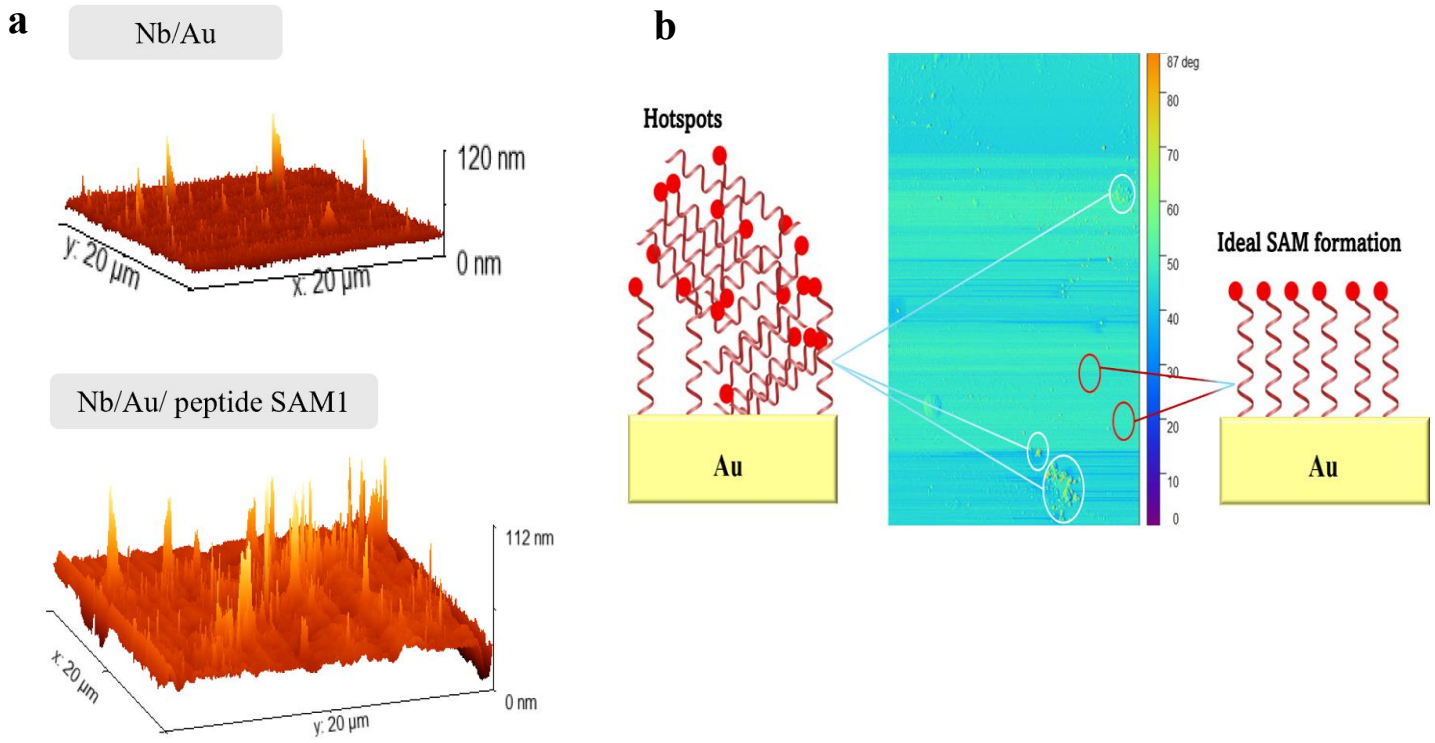



**Figure 6. a) 3D AFM images before/after peptide coverage. b) The variation of peptide coverage across gold surfaces.**

The bare Nb/Au exhibits a relatively smooth morphology with isolated protrusions. After coating with the peptide SAM, the surface displays higher and more frequent peaks, indicating an overall increase in nanoscale roughness and the formation of peptide-rich domains.

Relation to coverage heterogeneity.

Figure( 6b) summarizes how substrate features influence peptide organization. Local "hot spots" (topographic protrusions or high-energy sites) favor preferential

adsorption and clustering, whereas flatter terraces promote more uniform, near-ideal SAM formation. The schematic/heat map emphasizes that spatial variations in peptide coverage correlate with underlying surface morphology.

The AFM measurements reveal clear differences between the bare Nb/Au substrate and the peptide-coated samples (Table 1). The Nb/Au surface exhibited a very low thickness of 0.82 nm and relatively smooth morphology, with roughness values of Sq = 1.85 nm and Sa = 1.33 nm. After deposition of the peptide layer (SAM1), the thickness increased markedly to 186.5 nm, while the roughness values also rose (Sq = 7.96 nm, Sa = 3.48 nm), indicating successful film formation and the development of nanoscale heterogeneity across the surface.

Following PPMS analysis, the peptide films (SAM1–SAM3) retained higher roughness compared to the bare Nb/Au surface but displayed reduced Sq values in the range of 3.69–5.19 nm and Sa values between 1.86–3.67 nm. This reduction suggests that the peptide layers underwent partial rearrangement and smoothing, while still maintaining continuous coverage. The results confirm that peptide assembly significantly alters the topography of Nb/Au substrates and that subsequent processing influences the degree of surface organization.

**Table 1. Summary of data for 20 µm × 20 µm samples deposited on Nb/Au.**

| Sample | Thickness | RMS roughness (Sq) | Mean roughness (Sa) |
|---|---|---|---|
| **Before PPMS** | | | |
| **Nb/Au** | 0.82 nm | 1.85 nm | 1.33 nm |
| **Nb/Au/peptide SAM1** | 186.5 nm | 7.96 nm | 3.48 nm |
| **After PPMS** | | | |
| **Nb/Au/peptide SAM1** | - | 5.19 nm | 3.11 nm |
| **Nb/Au/peptide SAM2** | - | 3.69 nm | 1.86 nm |
| **Nb/Au/peptide SAM3** | - | 4.39 nm | 3.67 nm |

The AFM analysis provided further insights into the nanoscale organization of the peptide-coated Nb/Au surface. The topographic map (7a), obtained after 2D FFT filtering, highlights the distribution of surface features, with manually labeled height values showing clear variability across the scanned region. This heterogeneity reflects the presence of distinct peptide domains and local clustering on the substrate. The statistical evaluation of these features is presented in the histogram (7b), which shows the distribution of particle heights fitted with a Gaussian function. The data yielded a mean particle height of 29 nm with a standard deviation of 17.2 nm, indicating a broad range of vertical dimensions. Such variability suggests the coexistence of smaller peptide aggregates and larger domains, consistent with the self-assembly process on gold substrates. Together, the AFM topography and the height distribution confirm that the peptide forms a continuous but structurally heterogeneous film, in line with the roughness parameters reported earlier

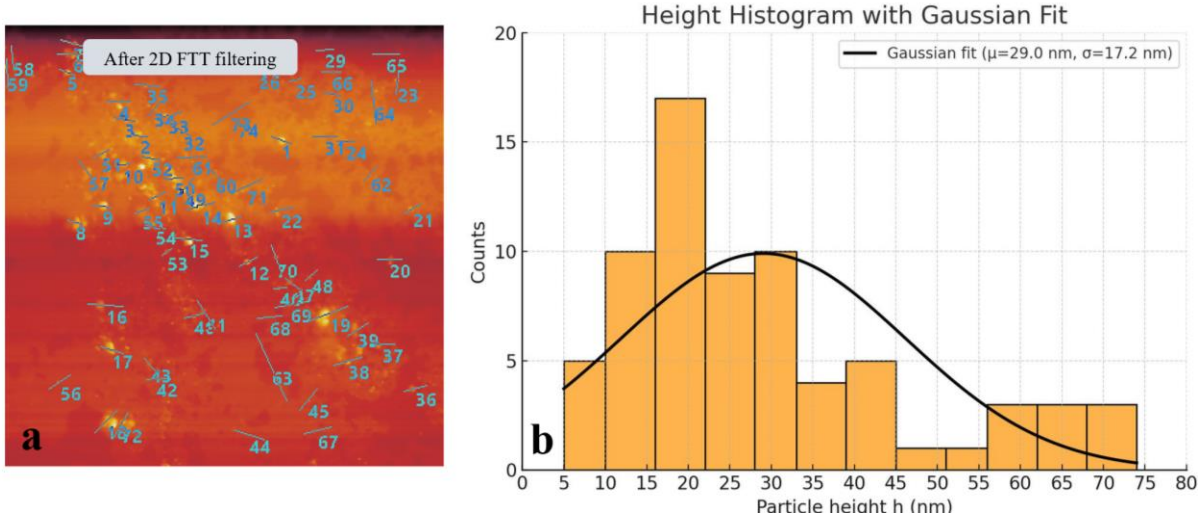



**Figure 7. a) AFM image of a 1 mmol sample deposited on Nb/Au, with height values manually labelled in blue. (b) Histograms showing the distribution of particle heights across the sample, with a Gaussian fit used to estimate the mean and standard deviation.**

## 4.2.3 Physical Property Measurement System (PPMS)

The resistance versus temperature curves under applied magnetic fields are shown in Figure 7. For the bare Nb/Au sample, the superconducting transition occurs at ~6.1 K and shifts gradually to lower temperatures as the magnetic field increases,

consistent with typical type-II superconducting behavior. When the Nb/Au films are coated with peptide SAMs (SAM1–SAM3), similar transitions are observed, and the effect of the magnetic field remains qualitatively the same. This confirms that the presence of peptide layers does not suppress the superconducting state of the Nb/Au films.

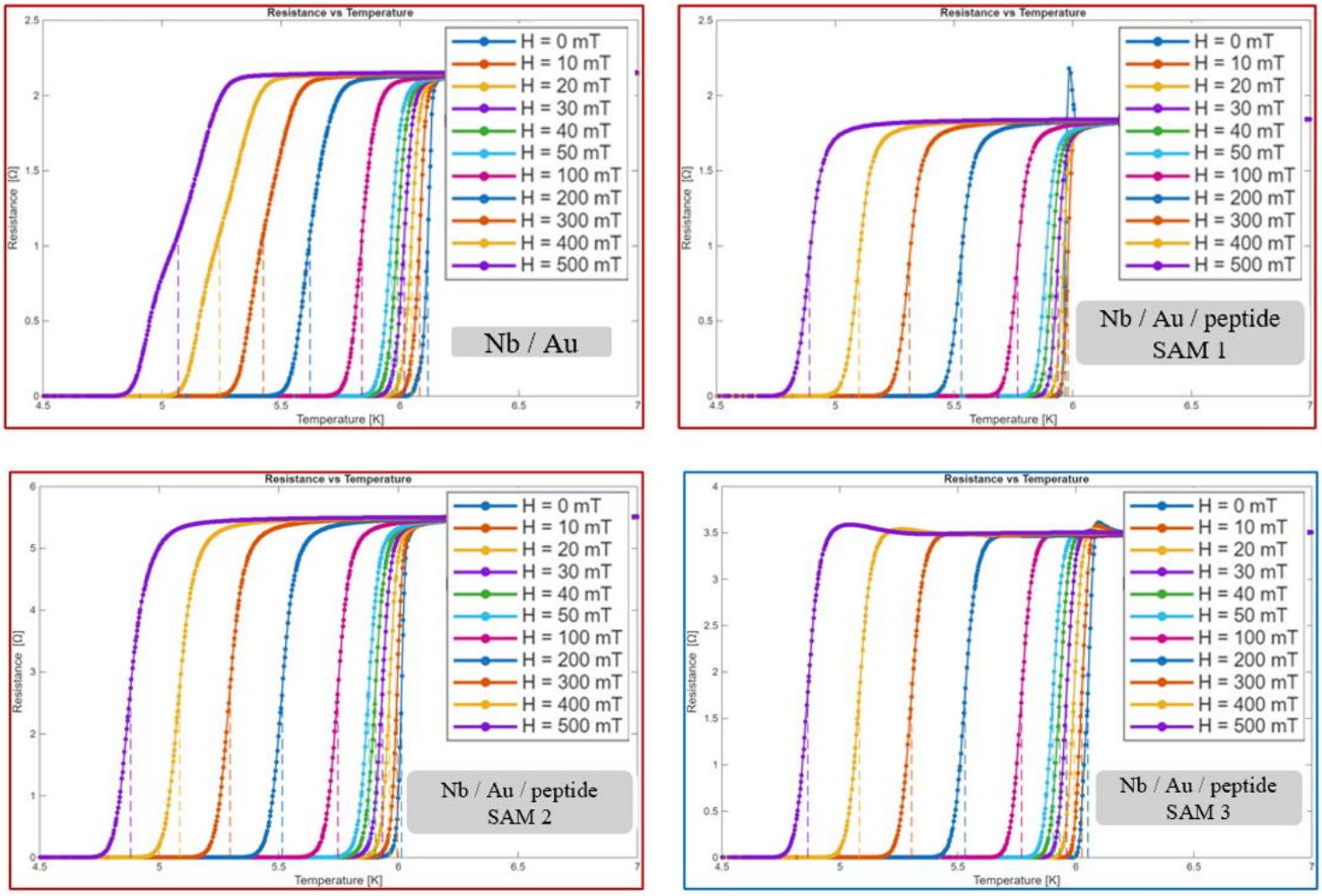



**Figure 7. Resistance as a function of temperature under different out-of-plane magnetic fields (red frame) and in-plane magnetic fields (blue frame).**

A direct comparison of the zero-field resistance transitions for all samples is presented in Figure 8. The transitions occur within a narrow range between 5.97 K and 6.12 K, with only minor variations between the bare Nb/Au and peptide-coated samples. This further demonstrates that the superconducting critical temperature is essentially preserved after peptide functionalization.

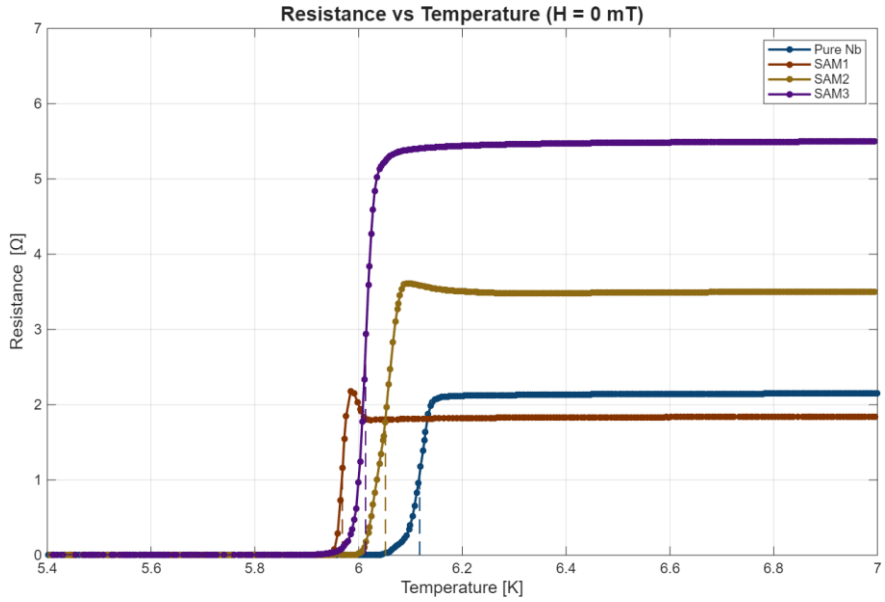



**Figure 8. Resistance as a function of temperature under H=0 mT magnetic fields.**

The extracted superconducting parameters are summarized in Table 2. The critical temperature Tc(0) was measured as 6.12 K for bare Nb/Au and between 5.97–6.05 K for peptide-coated samples, while the coherence length $\xi(0)$ varied slightly from 11.8 to 12.35 nm. These results highlight that peptide SAM deposition introduces only subtle modifications to the superconducting parameters, thereby confirming that the bio-organic layers are compatible with Nb/Au superconducting surfaces.

**Table 2. Superconducting $T_c$ (0) and $\xi$ (0) for bare Nb/Au and Nb/Au films coated with chiral peptide SAMs.**

| Sample | $T_c$ (0) | Coherence Length $\xi$ (0) |
|---|---|---|
| **Nb / Au** | 6.12 K | 12.5 nm |
| **Nb / Au / peptide SAM 1** | 5.97 K | 12.35 nm |
| **Nb / Au / peptide SAM 2** | 6.05 K | 11.8 nm |
| **Nb / Au / peptide SAM 3** | 6.01 K | 12.07 nm |

## 5. Challenges and Future

At the beginning of the internship, we had some difficulty using new software (such as Gwyddion and Nanoscope) to analyze the scans and readings we extracted from the AFM, which we also had to learn how to operate from scratch. It was an enriching challenge, as we ended our experience with newfound confidence and knowledge. We also had some issues with accessing the lab at the start of the internship, so it took longer than usual for us to obtain our results. For the future, we hope to have more time to work with chiral molecules and how they display the CISS effect on superconductors, especially if it's a molecule that's similar to the peptide we examined for this research project.

## 6. Resources and Tools

The experimental work for this study was carried out primarily at the Blackett Laboratory, Imperial College London, with additional film deposition conducted at the Department of Materials Science and Metallurgy, University of Cambridge. For sample characterization, atomic force microscopy (AFM) measurements were performed, supported by a Physical Property Measurement System (PPMS) for transport and magnetic response analysis, and pulsed laser deposition (PLD) for thin-film fabrication. Data processing and visualization were conducted using MATLAB, Gwyddion, and Nanoscope software.

In addition to experimental resources, the Abdus Salam Library at Imperial College provided access to key literature, including recent reviews and research articles on chiral-induced spin selectivity and its implications in superconducting systems, as well as the fundamentals needed for this project like an introduction to surface and thin-film growth. These resources informed the theoretical framework and contextual understanding for this work.

## 7. Reference

[1] B. P. Bloom, Y. Paltiel, R. Naaman, and D. H. Waldeck, “Chiral Induced Spin Selectivity,” Chem. Rev., vol. 124, no. 4, pp. 1950–1991, Feb. 2024, doi: 10.1021/acs.chemrev.3c00661.

[2] N. Sukenik et al., “Imprinting Chirality on a Conventional Superconductor,” Advanced Physics Research, vol. 2, no. 4, Jan. 2023, doi: 10.1002/apxr.202200072.

[3] R. Naaman, Y. Paltiel, and D. H. Waldeck, “Chiral Induced Spin Selectivity and Its Implications for Biological Functions,” Annu. Rev. Biophys., vol. 51, no. 1, pp. 99–114, May 2022, doi: 10.1146/annurev-biophys-083021-070400.

[4] C. Guo et al., “Extensive photochemical restructuring of molecule-metal

surfaces under room light,” Nat Commun, vol. 15, no. 1, Mar. 2024, doi:10.1038/s41467-024-46125-x.

[5] O. R. Bolduc, C. M. Clouthier, J. N. Pelletier, and J.-F. Masson, “Peptide Self-

Assembled Monolayers for Label-Free and Unamplified Surface Plasmon Resonance Biosensing in Crude Cell Lysate,” Anal. Chem., vol. 81, no. 16, pp.

6779–6788, July 2009, doi: 10.1021/ac900956y.